Journal of Alloys and Compounds 864 (2021) 158200

Contents lists available at ScienceDirect

Journal of Alloys and Compounds

journal homepage: www.elsevier.com/locate/jalcom

Full length article

Magnetization reversal and sign reversal exchange bias field in polycrystalline $Ni_{5.33}Ta_{0.67}B_2O_{10}$

S.N. Sofronova[a,*], N.V. Kazak[a], E.V. Eremin[a], E.M. Moshkina[a], A.V. Chernyshov[a,b], A.F. Bovina[a]

[a] Kirensky Institute of Physics, Federal Research Center KSC SB RAS, 660036 Krasnoyarsk, Russia
[b] Siberian State University of Science and Technologies, 660014 Krasnoyarsk, Russia

ARTICLE INFO

Article history:
Received 18 September 2020
Received in revised form 30 November 2020
Accepted 1 December 2020
Available online 7 December 2020

Keywords:
Exchange bias
Quasi low-dimensional compounds
Frustrated magnetism
Magnetisation reversal

ABSTRACT

The sign reversal of both magnetization and exchange bias field was studied in the polycrystalline $Ni_{5.33}Ta_{0.67}B_2O_{10}$. The crystal structure of $Ni_{5.33}Ta_{0.67}B_2O_{10}$ is quasi–low dimensional due to NiO_6/TaO_6 octahedra forming two dimensional infinite layers. The antiferromagnetic/ferrimagnetic phase transition was observed at T_N = 165 K. The negative exchange bias effect was found in the 30–90 K temperature range, whereas the positive exchange bias effect was observed at temperatures below 30 K. We assume that the exchange bias effect is due to different types of magnetic ordering of Ni^{2+} magnetic moments in two layers.

1. Introduction

Phenomena of the magnetization reversal and exchange bias are considered to be quite an intriguing aspect of magnetism. Both effects can be used for practical application in magnetic memory. The magnetization reversal is observed in compounds with complex magnetic structure, for example, ferrimagnet with negative exchange coupling among ferromagnetic sublattices [1]. The exchange bias effect usually occurs in ferromagnetic and antiferromagnetic bilayers or multilayers [2–5]. There is an effect of the sign reversal of exchange bias depending on the cooling field, temperature and other external parameters [6–8]. There are many single-phase alloys and compounds in which both sign reversal magnetization and sign reversal exchange bias are observed [7–10]. Most of them are oxides and have a perovskite or perovskite-like crystal structure [7–11], but some of them have spinel and other crystal structure [12,13].

For different compounds various mechanisms have been proposed for the origin of the exchange bias and magnetization reversal. Thus, in core-shell type $La_{0.2}Ce_{0.8}CrO_3$ nanoparticles the sign of the magnetization and exchange bias changes at the same temperature, which is a compensation point (T_{comp}) [8]. The authors [8] assume that the sign of the exchange bias in $La_{0.2}Ce_{0.8}CrO_3$ depends on the interface exchange coupling, which is in accordance with the suggestion of *Nogues* in [14] that the positive exchange bias could occur if the interface exchange coupling is antiferromagnetic, whereas the negative exchange bias could be observed if the interface exchange coupling is ferromagnetic. Below T_{comp}, the antiferromagnetic interface exchange coupling between the shell magnetization and Ce moments predominates, whereas above T_{comp}, the ferromagnetic interface exchange coupling between the magnetization shell and Cr moments is dominant.

In $NdMnO_3$, the Mn^{3+} and Nd^{3+} sublattices have different types (canted AFM and FM, respectively) and temperatures (79 and 13 K, respectively) of magnetic ordering [10]. The ferromagnetic sublattice of Nd^{3+} and ferromagnetic component of the Mn^{3+} sublattice are antiferromagnetically coupled, which provides possibility for the exchange bias effect to occur. The sign of exchange bias effect depends on the coupling intensity between the Nd ordering and Mn ferromagnetic component.

In the polycrystalline Er_2CoMnO_6 the exchange bias effect can occur due to the pinning at the interface of ordered and antisite disordered phases [11]. In ordered phase, Co ions occupy 2c position while Mn ions occupy 2d position. In antisite disordered phase, Co and Mn positions are interchanged Co(2d)-Mn(2c). It is assumed that in ordered phase the Er moments are arranged ferromagnetically at the interface, whereas in antisite disordered phase they are arranged antiferromagnetically [11]. A weak AFM interfacial correlation between the ordered and antisite disordered phases leads to the negative exchange bias.

In the polycrystalline $YbCr_{1-x}Fe_xO_3$ [15], $Co(Cr_{0.9}Fe_{0.1})_2O_4$ [12] and in $TmCrO_3$ [16] the sign reversal of exchange bias field originated

* Corresponding author.
E-mail address: ssn@iph.krasn.ru (S.N. Sofronova).

https://doi.org/10.1016/j.jallcom.2020.158200
0925-8388/

from the spin reorientation of the sublattice magnetic moments and the unidirectional anisotropy.

The zero field exchange bias effect is also very intriguing. This effect was found in Ni-Mn-In bulk alloys after zero-field cooling from an unmagnetized state [17]. The zero-field exchange bias effect together with magnetization reversal was found in $CuCr_{1-x}Mn_xO_2$ [13] and in $La_{1.5}Sr_{0.5}Co_{0.4}Fe_{0.6}MnO_6$ [18]. In the polycrystalline $Y_{0.9}Pr_{0.1}CrO_3$, the zero-field exchange bias effect was claimed to be due to the superposition of the frozen magnetic domains and unidirectional anisotropy developed at the interfaces of the domains [19].

Oxyborates are very perspective compounds for such effects as exchange bias and magnetization reversal due to low-dimensional elements in the crystal structure. The investigation of Ni-based oxyborates showed that the doping $Ni_3B_2O_6$ with kotoite structure [20] by magnetic or nonmagnetic ions leads not only to the changing crystal structure but also to interesting magnetic properties. When Ni ions are substituted with trivalent Mn ions, the crystal structure changes to ludwigite crystal structure and the magnetization reversal occurs in $(Ni,Mn)_3BO_5$ [21]. We assume that the magnetization reversal in $(Ni,Mn)_3BO_5$ is attributed to two magnetic subsystems which are coupled antiferromagnetically. The exchange bias effect occurs in $Ni_5GeB_2O_{10}$ [22] with ludwigite crystal structure where the Ni ions are substituted with nonmagnetic tetravalent Ge ions. In this paper we present the study of the sign reversal of magnetization and exchange bias in the polycrystalline compound $Ni_{5.33}Ta_{0.67}B_2O_{10}$. In this compound some Ni ions are substituted with pentavalent Ta ions. This material was reported in 1990 by Bluhm [23] who studied its crystal structure and presented the measurements of the reciprocal magnetic susceptibility.

$Ni_{5.33}Ta_{0.67}B_2O_{10}$ has a specific crystal structure, with the NiO_6/TaO_6 octahedra forming two- dimensional infinite layers (Fig. 1a and b). The metallic ions occupy eight crystallographic positions in layers and between layers [23] (Table 1). In the first layer (Layer I), both metallic ions of Ni and Ta (green and grey circles on Fig. 1a, respectively) are ordered in their own crystallographic positions, thereby forming the triangular arrangement of magnetic ions. In the second layer (Layer II), there are two crystallographic positions, which are occupied both by Ni and Ta ions in different proportions (the magenta circles in Fig. 1b), and one position is fully occupied by Ni. In this layer the exchange ways form a lattice, which is very close to the square one (Fig. 1b). Layers I and II are connected by the NiO_6 octahedra (Ni I in Fig. 1) through corners and edges, respectively. Such a layered crystal structure provides the basis for the magnetization reversal and exchange bias if the magnetic orderings of alternating layers are ferromagnetic/antiferromagnetic.

It is interesting to note that the appearance of a variety of magnetic interactions in the complicated crystal structures leads to an increase in the temperature of magnetic ordering from 49 K in $Ni_3B_2O_6$ [20] to 87 K in $Ni_5GeB_2O_{10}$ [22] and 165 K in $Ni_{5.33}Ta_{0.67}B_2O_{10}$ [23]. In all these compounds only the Ni ions are magnetic ones but these magnetic ions form different low-dimensional elements which are ribbons in $Ni_3B_2O_6$, zig-zag walls in $Ni_5GeB_2O_{10}$ or $(Ni,Mn)_3BO_5$ and layers in $Ni_{5.33}Ta_{0.67}B_2O_{10}$. It is interesting to investigate the magnetic properties of $Ni_{5.33}Ta_{0.67}B_2O_{10}$ in detail because the temperature of magnetic transition is high but only the measurements of the reciprocal magnetic susceptibility were previously presented [23].

2. Synthesis and structural characterization

Single crystals of $Ni_{5.33}Ta_{0.67}B_2O_{10}$ were synthesized by the flux method. The ratio of the initial oxides was $Bi_2Mo_3O_{12}$:2.55B_2O_3:2Li_2O:0.72NiO:0.045Ta_2O_5. The flux with a weight of 91.6 g was prepared in a platinum crucible (V=100 cm^3) at the temperature T = 1100 °C by sequential melting of the powder components. The sequence of melting was the following: Bi_2O_3, MoO_3 and B_2O_3 oxides were mixed; then, NiO oxide and Ta_2O_3 oxide were successively added; and finally, Li_2CO_3 carbonate was added in portions (during the heating up to T = 1100 °C the reaction $Li_2CO_3 \rightarrow Li_2O+CO_2\uparrow$ proceeded). After the melting process, the flux was homogenized for 3 h at T = 1100 °C.

Single crystals of $Ni_{5.33}Ta_{0.67}B_2O_{10}$ were obtained by spontaneous nucleation. After the homogenization stage the temperature in the furnace was first rapidly decreased down to 960 °C and then, slowly

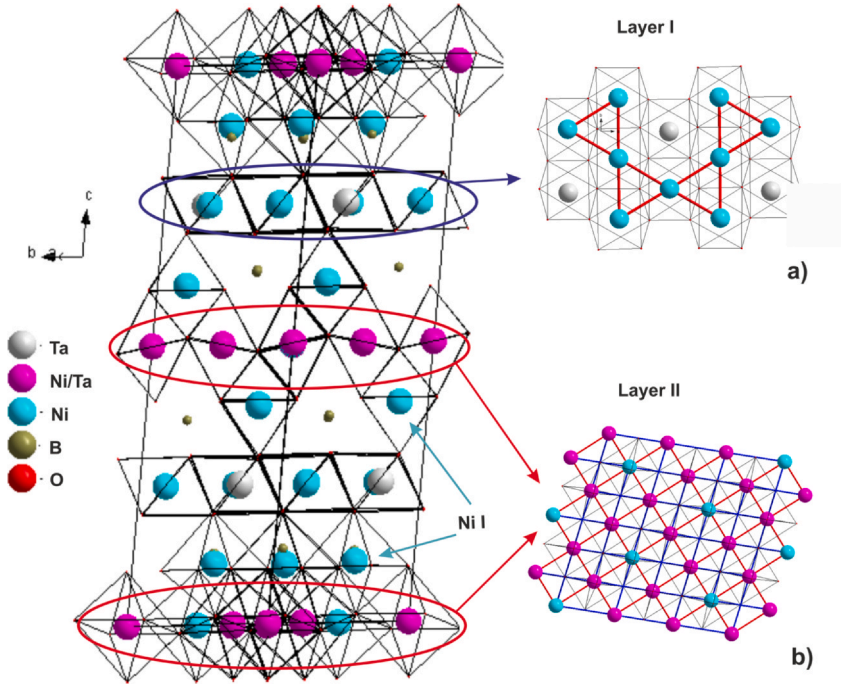

Fig. 1. The crystal structure of $Ni_{5.33}Ta_{0.67}B_2O_{10}$. Fig. a and b show layer I and layer II, respectively.

Table 1
The metallic ions coordinates taken from [23]:.

Ions	Position	Occupation	x	y	z	
Ni_1/Ta_1	8f	0.875/0.125	0.3749(5)	0.1265(8)	0.4991(8)	Layer I
Ni_2	8f	1	0.2507(5)	0.0676(8)	0.2502(2)	Layer II
Ni_3	8f	1	0.6090(4)	0.1874(8)	0.6092(2)	Ni I
Ni_4	8f	1	0.1425(5)	0.0611(8)	0.3928(2)	Ni I
Ni_5/Ta_5	4a	0.915/0.085	0	0	0.5	Layer I
Ni_6	4c	1	0.75	0.25	0.5	Layer I
Ni_7	4e	1	0	0.8132(12)	0.25	Layer II
Ta	4e	1	0.5	0.2127(5)	0.75	Layer II

reduced at a rate of 24 °C/day. 24 h later, the crucible was withdrawn from the furnace, and the flux was poured out. The single crystals grown in the form of black parallelogram plates with the size of about 0.5 * 0.5 mm2 were etched in a 20% aqueous solution of nitric acid to remove the flux residue.

The x-ray diffraction measurements have been done at room temperature using a D8 ADVANCE diffractometer with a Vantec detector (CuKa radiation, λ = 1.5406 A °, scanning angle 2θ=5–90º). The x-ray diffraction data revealed the hulsite-type structure with lattice parameters a = 10.5560 Å, b = 6.1463 Å, c = 21.6314 Å, β = 101.820º, and V= 1373.70 Å3.

3. Results

The magnetic properties were investigated on polycrystalline samples using a commercial PPMS 6000 platform (Quantum Design). Fig. 2 shows the temperature dependences of magnetization in the zero-field-cooled (ZFC), field-cooled (FC), and field-cooled-heating (FCH) conditions measured at H= 200 Oe.

The ZFC curve displays a clear feature at T_N = 165 K which is accompanied by the thermal hysteresis of FC and FCH magnetizations. The observed anomaly can be attributed to the onset of (antiferro)ferrimagnetic order of the Ni^{2+} magnetic moments. Upon further cooling the next anomalies are revealed with larger thermal hysteresis and magnetization kinks at 50 and 30 K (Fig. 2). The ZFC curve crosses the M= 0 axis twice: at around T_{comp1}= 163 and T_{comp2}= 30 K remaining negative in this range. The FC and FCH curves cross the M= 0 axis and turn negative below T_{comp2}. The paramagnetic moment 7,02 μB/f.u. was estimated from the fit of the magnetic susceptibility in field 1 kOe and temperature range of 220–250 K, which corresponds to the theoretical spin moment of 6,53 μB. The paramagnetic Curie temperature was found to be − 26 K, indicating the antiferromagnetic interaction between the spins.

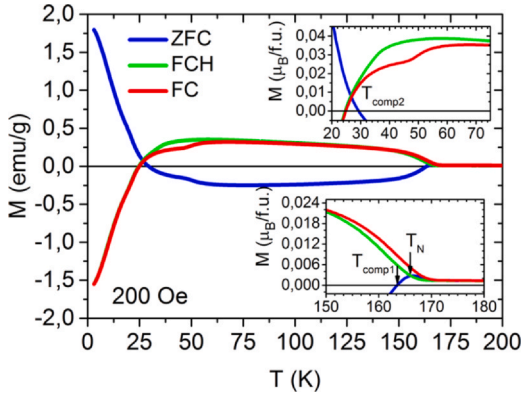

Fig. 2. The magnetization in the zero-field-cooled (ZFC), field-cooled (FC), and field-cooled-heating (FCH) conditions measured at H= 200 Oe. The bottom inset shows a magnetic anomaly associated with the magnetic phase transition at T_N and high-temperature compensation point T_{comp1}. The top inset displays the kinks of FC and FCH magnetizations and low-temperature compensation point T_{comp2}.

The magnetization reversal is also present in fields 1 kOe and 2 kOe, it disappears at higher fields. Under a field higher than 2 kOe the magnetization monotonically increases with the decreasing temperature. We measure the temperature dependence of magnetization at − 1 kOe in order to eliminate the effect of a stray field on the magnetization reversal phenomenon. M(+1 kOe) equals to –M(-1 kOe). The thermal hysteresis at around 50 K between the FC and FCH data at different fields is not given. But the irreversibility between FC and FCH is present even at 10 kOe, and it almost vanishes at 15 kOe.

Fig. 3 shows the isothermal M(H) data recorded in the FC regime (H_{cool} = 1 kOe) at different temperatures. Here, the shape of the hysteresis loop as well as the sign of the exchange bias depend on temperature. The weak exchange bias of the hysteresis loop appears below 100 K and it is negative (H_{eb}) (NEB in Fig. 4). Below 40 K, H_{eb} increases in absolute value and changes its sign to positive at about 26 K(PEB in Fig. 4), which is close to the temperature of compensation T_{comp2}.

The shape of the hysteresis loop changes several times. First, the hysteresis loop changes its shape at 125 K (Fig. 3d). At this temperature the coercive field (H_c) has maximum (Fig. 4). With the decreasing temperature the hysteresis loop shape changes again and in the temperature range of 50–100 K there are no significant changes (Fig. 3c). Below 40 K, the hysteresis loop changes its shape again and H_{eb} increases. Near the temperature of compensation T_{comp2}= 26 K the loops are thin, H_c is almost zero (Fig. 3b). With the decreasing temperature the coercive field (H_c) and positive exchange bias are increased (Fig. 3b and Fig. 4).

We calculated the first derivatives of both descending and ascending branches of the loops to determine whether hysteresis loops are minor or saturated ones [24]. The first derivatives of both the descending and ascending branches coincide in the range of 85 – 90 kOe for the hysteresis loops in the temperature range of 10 – 100 K. For the hysteresis loop measured at 5 K the derivatives coincide in the range of 75 – 90 kOe. We assume that the shift of the hysteresis loops along the H-axis is due to the exchange bias effect.

We measured the isothermal M(H) at 5 K under different cooling fields. As it is shown in Fig. 5a the exchange bias field depends only slightly on the positive cooling fields. The measurements in the positive and negative cooling fields showed that after cooling in the positive field of 90 kOe the exchange bias is positive (green line in Fig. 5b), after cooling in the negative field of − 90 kOe the exchange bias is negative (red line in Fig. 5b), which is similar to the behavior of the exchange bias found in Er_2CoMnO_6 [10]. We did not observe the zero-field exchange bias in the given compound.

We conclude that in $Ni_{5.33}Ta_{0.66}B_2O_{10}$ the magnetization reversal is observed in weak fields, and the sign reversal exchange bias depends on temperature. The exchange bias field changes its sign close to the temperature of compensation T_{comp2}.

4. Analysis and discussion

We carried out the theoretical group analysis and the empirical calculation of the super exchange interactions. It is clear that for

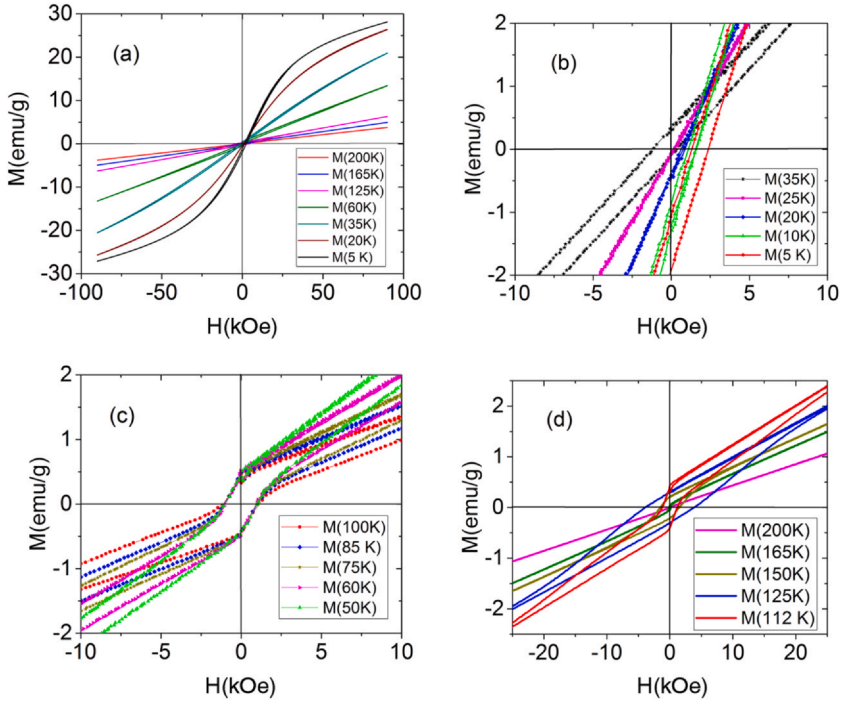

Fig. 3. (a) The M-H hysteresis loops measured at different temperatures in the FC condition (H_{cool}=1 kOe). The enlarged hysteresis loops in different temperature ranges: 5–35 K (b), 50–100 K (c), 112–200 K (d).

chemically disordered compounds the symmetry law can be violated; however, the theoretical group analysis provides a number of the background magnetic states. The analysis was performed for the $C_{12/c1}$ symmetry group. We consider the case in which the magnetic cell coincides with the crystallographic one. Magnetic representation is constructed for each element of the symmetry. Then, for these magnetic representations, the decomposition of reducible representations into irreducible representations is calculated (Eq. 1), the projection operator is constructed and its eigenvectors are calculated (Table 2).

$$D(k=0) = \mathbf{33}\tau_1 + \mathbf{33}\tau_2 + \mathbf{33}\tau_3 + \mathbf{33}\tau_4 \quad (1)$$

The super exchange interactions were estimated using a simple indirect coupling model [25,26] based on the theory of the super exchange interaction [27,28]. The details of similar calculations are presented in paper and supplementary data [29]. The calculated exchange integrals for $Ni_{5.33}Ta_{0.67}B_2O_{10}$ are presented in Table 1. Here, b and c are the electron transfer parameters being squares of the ligand-cation intermixing coefficients for the σ and π coupling, respectively (the values of these parameters are b=0.02 and c=0.01); U_{Ni}= 2.7 eV is the cation-ligand excitation energy [30]; J^{in} = 1,87 eV is the integral of the interatomic exchange interaction [31].

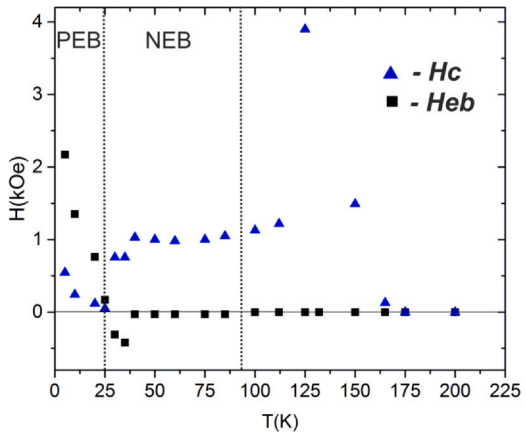

Fig. 4. The coercive field (H_c) and exchange bias field (H_{eb}) as a function of temperature, where PEB is the positive exchange bias and NEB is the negative exchange bias.

Three types of the superexchange interactions were obtained which are ferromagnetic J^{90°, and antiferromagnetic J^{180° and J^{120°. The values of the superexchange interaction Ni_i-Ni_j are showed in Table 3 and they depend on the occupation of the i-th and j-th positions taken from Table 1.

We found that all the superexchange interactions between the Ni^{2+} ions in layer I are ferromagnetic J^{90°(the red line in Fig. 1a), while both ferromagnetic J^{90° and antiferromagnetic J^{180° exchange interactions (the red and blue lines in Fig. 1b, respectively) are present in layer II. The exchange interactions between Ni I and layer I are antiferromagnetic (J^{120°), while those with layer II are ferromagnetic (J^{90°).

Based on the theoretical group analysis and calculated exchange interactions we estimated the energy of different ordered magnetic structures in the framework of the mean field theory (Eq. 2, Table 4). We took into account the simple model where the magnetic moments of ions have spins directed up or down (u and d in Table 4, respectively). The direction of magnetic moments of ions, which belong to the same crystallographic position corresponds to the ferromagnetic or antiferromagnetic component of the eigenvectors (Table 2). The expression of energy in terms of the exchange interactions is presented in Table 4.

$$E = -\frac{1}{2}\sum_{ij} S_i S_j J_n \quad (2)$$

The magnetic structure shown in Fig. 6 is characterized by the lowest energy value. As can be seen, the magnetic moments in layer I are ferromagnetically ordered, but in layer II there is an antiferromagnetic ordering. The magnetic moments of Ni I are antiferromagnetically ordered towards layer I. The exchange interactions in layer II are frustrated, and some exchange interactions between Ni

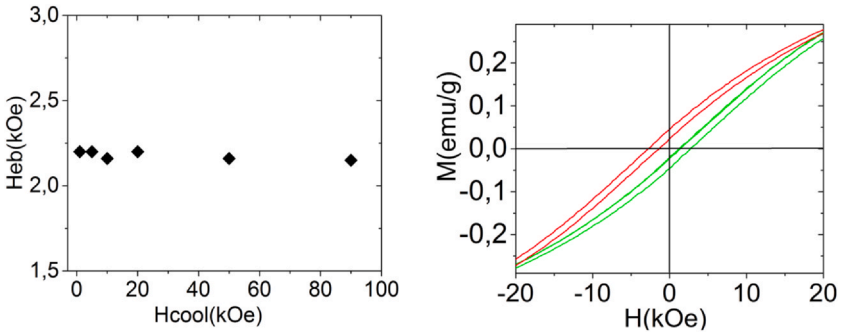

Fig. 5. The exchange bias field (H_{eb}) as a function of the cooling field (H_{cool}).

Table 2
The eigenvectors for irreducible representations.

Position	τ_1	τ_2	τ_3	τ_4
8f	x y z	x y z	x y z	x y z
	-x -y z	-x -y z	x y -z	x y -z
	x y z	-x -y -z	x y z	-x -y -z
	-x -y z	-x -y z	x y -z	-x -y z
	x y z	x y z	x y z	x y z
	-x -y z	-x -y z	x y -z	x y -z
	x y z	-x -y -z	x y z	-x -y -z
	-x -y z	-x -y z	x y -z	-x -y z
4c	x y z	x y z	x y z	x y z
	-x -y z	-x -y z	x y -z	x y -z
	x y z	-x -y -z	x y z	-x -y -z
	-x -y z	x y -z	x y -z	-x -y z
4a	x y z	0 0 0	x y z	0 0 0
	-x -y z	0 0 0	x y -z	0 0 0
	x y z	0 0 0	x y z	0 0 0
	-x -y z	0 0 0	x y -z	0 0 0
4e	x y z	0 0 0	x y z	0 0 0
	-x -y z	0 0 0	x y -z	0 0 0
	x y z	0 0 0	x y z	0 0 0
	-x -y z	0 0 0	x y -z	0 0 0

I and layer II are frustrated as well. Such magnetic ordering can lead to the exchange bias effect. Nevertheless, the magnetization reversal effect is experimentally observed at T_{comp2} around 26 K and the exchange bias effect changes its sign at around 30 K.

In the model proposed in [2] for the exchange bias effect to be observed the ferromagnetic layer needs to be ordered first, which will influence the ordering of antiferromagnetic layer. The magnetization reversal can be observed when there are two magnetic subsystems which are coupled antiferromagnetically. We suggest that in $Ni_{5.33}Ta_{0.67}B_2O_{10}$ there should be several magnetic subsystems and thus, we propose two possible models of magnetic subsystems. In both models there are two ferromagnetically ordered subsystems which are ordered first and coupled antiferromagnetically. The ordering of the third subsystem leads to the formation of antiferromagnetic layers and exchange bias effect.

The first model includes three magnetic subsystems. The first subsystem is layer I, which is ordered ferromagnetically. Layer II and Ni I chains are the second and third subsystems, respectively (Fig. 6 Model I). Ni I chains are also ordered ferromagnetically. In this case, the magnetic ordering in subsystems I and III is formed at around 165 K. The magnetization reversal appears due to the antiferromagnetic exchange interactions between subsystems I and III.

Table 3
The calculated exchange integrals for $Ni_{5.33}Ta_{0.67}B_2O_{10}$.

Ni_i-Ni_j	Angles	J_n	Expression	n_i	n_j	J_n (K)
Ni_7-Ni_2	α = 91° β = 94°	J_5	$J^{90°} = \frac{2}{3}bcJ^{in}(sin\alpha + sin\beta)n_in_j$	1	1	5.8
Ni_7-Ni_2	α = β = 95°	J_6		1	1	5.8
Ni_3-Ni_5	α = 98° β = 94°	J_8		1	0.915	5.3
Ni_3-Ni_6	α = 93° β = 98°	J_{11}		1	1	5.8
Ni_3-Ni_1	α = 95° β = 97°	J_{12}		1	0.875	5.1
Ni_3-Ni_1	α = 99° β = 92°	J_{13}		1	0.875	5.1
Ni_1-Ni_4	α = 92° β = 96°	J_{16}		0.875	1	5.1
Ni_1-Ni_4	α = 98° β = 92°	J_{19}		0.875	1	5.1
Ni_4-Ni_6	α = 92° β = 96°	J_{24}		1	1	5.8
Ni_4-Ni_5	α = 97° β = 93°	J_{25}		1	0.915	5.3
Ni_2-Ni_2	α = 96° β = 98°	J_1		1	1	5.8
Ni_3-Ni_4	α = β = 93°	J_9		1	1	5.8
Ni_3-Ni_4	α = 94° β = 93°	J_{10}		1	1	5.8
Ni_1-Ni_6	α = β = 81°	J_{20}		0.875	1	5.1
Ni_1-Ni_5	α = 82° β = 81°	J_{21}		0.875	0.915	4.6
Ni_1-Ni_1	α = β = 96°	J_{22}		0.875	0.875	4.4
Ni_1-Ni_1	α = β = 97°	J_{23}		0.875	0.875	4.4
Ni_6-Ni_5	α = 97° β = 96°	J_{26}		1	0.915	5.3
Ni_2-Ni_4	α = 120°	J_3	$J^{120°} = -\frac{8}{9}b^2U_{Ni} \mid cos\alpha \mid n_in_j$	1	1	-5.6
Ni_2-Ni_3	α = 115°	J_2		1	1	-4.7
Ni_2-Ni_3	α = 118°	J_4		1	1	-5.2
Ni_7-Ni_4	α = 120°	J_7		1	1	-5.6
Ni_1-Ni_6	α = 165°	J_{14}	$J^{180°} = -\frac{8}{9}b^2U_{Ni} \mid cos\alpha \mid n_in_j$	0.875	1	-9.3
Ni_1-Ni_6	α = 162°	J_{15}		0.875	1	-9.3
Ni_1-Ni_5	α = 166°	J_{17}		0.875	0.915	-8.6
Ni_1-Ni_5	α = 164°	J_{18}		0.875	0.915	-8.6

Table 4
The calculated energies of different magnetic structures.

	Ni_1 (8 f)	Ni_2 (8 f)	Ni_3 (8 f)	Ni_4 (8 f)	Ni_5 (4a)	Ni_6 (4c)	Ni_7 (4e)	Expression	*E (K)*
FIM_1	u	u	d	d	d	d	u	$-4*(J_1-2J_2-2J_3-2J_4-2J_5+2J_6-2J_7+2J_8+2J_9+2J_{10}+2J_{11}-2J_{12}-2J_{13}-2J_{14}-2J_{15}-2J_{16}-2J_{17}-2J_{18}-2J_{19}-2J_{20}-2J_{21}+J_{22}+J_{23}+2J_{24}+2J_{25}+J_{26})$	-564.9
FIM_2	d	u	d	d	d	d	u	$-4*(J_1-2J_2-2J_3-2J_4-2J_5+2J_6+2J_7+2J_8+2J_9+2J_{10}+2J_{11}+2J_{12}+2J_{13}+2J_{14}+2J_{15}+2J_{16}+2J_{17}+2J_{18}+2J_{19}+2J_{20}+2J_{21}+J_{22}+J_{23}+2J_{24}+2J_{25}+J_{26})$	-473.6
FIM_3	d	d	u	u	u	u	u	$-4*(J_1-2J_2-2J_3-2J_4-2J_5-2J_6+2J_7+2J_8+2J_9+2J_{10}+2J_{11}+2J_{12}-2J_{13}-2J_{14}-2J_{15}-2J_{16}-2J_{17}-2J_{18}-2J_{19}-2J_{20}-2J_{21}+J_{22}+J_{23}+2J_{24}+2J_{25}+J_{26})$	-382.5
FIM_4	u	d	u	u	d	u	u	$-4*(J_1-2J_2-2J_3-2J_4-2J_5-2J_6+2J_7-2J_8+2J_9+2J_{10}+2J_{11}+2J_{12}+2J_{13}+2J_{14}+2J_{15}+2J_{16}-2J_{17}-2J_{18}+2J_{19}+2J_{20}-2J_{21}+J_{22}+J_{23}+2J_{24}-2J_{25}+J_{26})$	-321.1
FIM_5	u	d	u	u	u	d	u	$-4*(J_1-2J_2-2J_3-2J_4+2J_5-2J_6+2J_7+2J_8+2J_9+2J_{10}-2J_{11}+2J_{12}+2J_{13}-2J_{14}-2J_{15}+2J_{16}+2J_{17}+2J_{18}+2J_{19}-2J_{20}+2J_{21}+J_{22}+J_{23}-2J_{24}+2J_{25}+J_{26})$	-414.8
FIM_6	d	u	u	u	u	u	d	$-4*(J_1+2J_2+2J_3+2J_4+2J_5-2J_6-2J_7+2J_8+2J_9+2J_{10}+2J_{11}-2J_{12}-2J_{13}-2J_{14}-2J_{15}-2J_{16}-2J_{17}-2J_{18}-2J_{19}-2J_{20}-2J_{21}+J_{22}+J_{23}+2J_{24}+2J_{25}+J_{26})$	-316.9
AFM_7	u	d	u	u	u	d	u	$-4*(-J_1+2J_2-2J_3-2J_4-2J_8+2J_9+2J_{10}+2J_{11}+2J_{12}+2J_{13}+2J_{15}+2J_{16}-2J_{17}-2J_{18}+2J_{19}+2J_{20}-2J_{21}+J_{22}+J_{23}+2J_{24}-2J_{25}+J_{26})$	-411.5
AFM_8	u	d	u	u	d	d	u	$-4*(-J_1+2J_2-2J_3-2J_4+2J_8+2J_9+2J_{10}+2J_{11}-2J_{12}+2J_{13}+2J_{15}+2J_{16}+2J_{17}+2J_{18}+2J_{19}+2J_{20}+2J_{21}+J_{22}+J_{23}+2J_{24}+2J_{25}+J_{26})$	-381.6

Due to frustrations, subsystem II is disordered, but with the decreasing temperature in this subsystem, ordered areas are formed, which leads to the exchange bias. The formation of different ordered areas can be due to the chemical disorder (Ni/Ta) in layer II. We assume that the formation of magnetic order in subsystem II at low temperature (at around 30 K) changes the sign of the exchange bias. It is in this temperature range (30–50 K) that the hysteresis between FC and FCH is observed.

The second model of magnetic subsystem of $Ni_{5.33}Ta_{0.67}B_2O_{10}$ can be presented as follows. The first subsystem is still Layer I. The second subsystem is a ribbon formed by the Ni I chains and portion of the Ni ions belonging layer II (Fig. 6 Model II). The third subsystem is the chains of the Ni ions in layer II which connect the ribbons with each other. The exchange interactions inside the ribbon are ferromagnetic and not frustrated. The exchange interactions between layer I and the ribbon are antiferromagnetic. The exchange interactions in subsystem I and II are ferromagnetic, whereas those between subsystem I and II are antiferromagnetic. All of these exchange interactions are not frustrated. In this case, only the exchange interactions between subsystem II and III are frustrated.

In the framework of the second model, the magnetic ordering in subsystems I and II is formed at 165 K. The magnetization reversal appears due to the antiferromagnetic exchange interactions between subsystem I and II. At around 100 K the exchange bias appears due to a part of the ions from subsystem III becoming ordered. In subsystem III the magnetic ordering is formed at around 30 K, which changes the sign of the exchange bias and behavior of H_c. The formation of the magnetic order in subsystem III and almost perpendicular orientation of the ribbons in the unit cell can affect the orientation of magnetic moments in the ribbons.

5. Conclusion

In conclusion, we have investigated the magnetic properties of polycrystalline $Ni_{5.33}Ta_{0.67}B_2O_{10}$. We have observed the magnetization reversal and sign reversal exchange bias effects. These effects have been found to depend on the temperature and field prehistory. The compound under study undergoes the antiferromagnetic/ferrimagnetic phase transition at T_N = 165 K. The theoretical group analysis and the empirical calculation of the super exchange interactions have been carried out, which reveals that the experimentally observed effects can be satisfactorily explained in the framework of two models of magnetic subsystems. Both models imply the existence of several magnetic subsystems formed by the Ni^{2+} ions. The complex crystallographic and magnetic structure makes it difficult to build a true model of magnetic ordering and to find an explanation for all the interesting features of the magnetic properties of $Ni_{5.33}Ta_{0.67}B_2O_{10}$. Nevertheless, it is necessary to continue studying the $Ni_{5.33}Ta_{0.67}B_2O_{10}$ single crystal because this compound is a perspective system for spintronic devices due to an

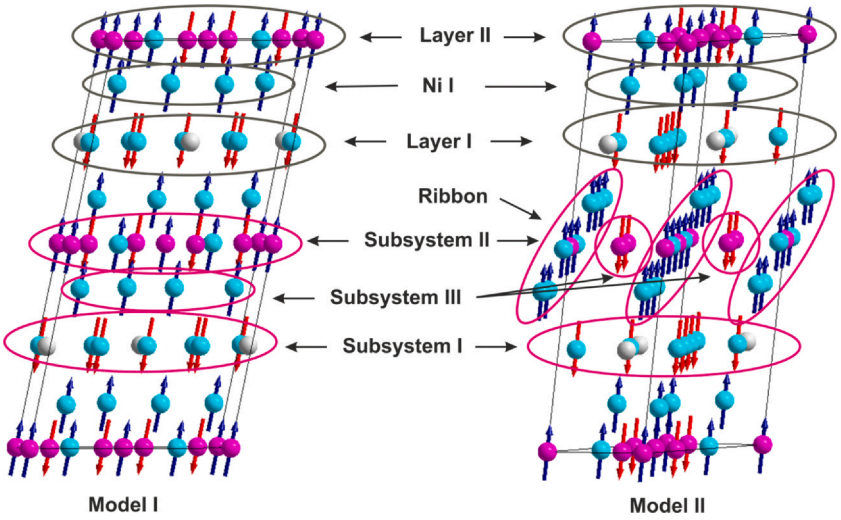

Fig. 6. The magnetic structure is characterized by the lowest energy value.

extraordinary coexistence of both the magnetization reversal and reversal exchange bias effects.

CRediT authorship contribution statement

S.N. Sofronova: Conceptualization, Writing - review & editing, Writing - original draft; **N.V. Kazak:** Conceptualization, Writing - review & editing; **E. V. Eremin:** Investigation, Validation; **E.M. Moshkina:** Investigation; **A.V. Chernyshov:** Formal analysis; **A. F. Bovina** – Investigation.

Declaration of Competing Interest

The authors declare that they have no known competing financial interests or personal relationships that could have appeared to influence the work reported in this paper.

Acknowledgments

The research was funded by RFBR, Krasnoyarsk Territory and Krasnoyarsk Regional Fund of Science, project number 18-42-240007.

The equipment of Krasnoyarsk Regional Center of Research Equipment of Federal Research Center “Krasnoyarsk Science Center SB RAS” was used for measurements in this research.

References

[1] A. Kumar, S.M. Yusuf, The phenomenon of negative magnetization and its implications, Phys. Rep. 556 (2015) 1–34.
[2] W.H. Meiklejohn, C.P. Bean, New magnetic anisotropy, Phys. Rev. 102 (1956) 1413–1414.
[3] J. Nogues, I.K. Schuller, Exchange bias, J. Magn. Magn. Mater. 192 (1999) 203–232.
[4] R.L. Stamps, Mechanisms for exchange bias, J. Phys. D Appl. Phys. 33 (2000) R247–R268.
[5] M. Kiwi, Exchange bias theory, J. Magn. Magn. Mater. 234 (2001) 584–595.
[6] K. Yoshii, Positive exchange bias from magnetization reversal in $La_{1-x}Pr_xCrO_3$(x~0.7–0.85), Appl. Phys. Lett. 99 (2011) 142501.
[7] T. Bora, S. Ravi, Sign reversal of magnetization and exchange bias field in $LaCr_{0.85}Mn_{0.15}O_3$, J. Appl. Phys. 114 (2013) 183902.
[8] P.K. Manna, S.M. Yusuf, R. Shukla, A.K. Tyagi, Coexistence of sign reversal of both magnetization and exchange bias field in the core-shell type $La_{0.2}Ce_{0.8}CrO_3$ nanoparticles, Appl. Phys. Lett. 96 (2010) 242508.
[9] R. Shukla, J. Manjanna, A.K. Bera, S.M. Yusuf, A.K. Tyagi, $La_{1-x}Ce_xCrO_3$(0.0 ≤x≤ 1.0): a new series of solid solutions with tunable magnetic and optical properties, Inorg. Chem. 48 (2009) 11691–11696.
[10] F. Hong, Z. Cheng, J. Wang, X. Wang, S. Dou, Positive and negative exchange bias effects in the simple perovskite manganite $NdMnO_3$, Appl. Phys. Lett. 101 (2012) 102411.
[11] A. Banerjee, J. Sannigrahi, S. Giri, S. Majumdar, Magnetization reversal and inverse exchange bias phenomenon in the ferrimagnetic polycrystalline compound Er_2CoMnO_6, Phys. Rev. B 98 (2018) 104414.
[12] C.L. Li, T.Y. Yan, G.O. Barasa, Y.H. Li, R. Zhang, Q.S. Fu, X.H. Chen, S.L. Yuan, Negative magnetization and exchange bias effect in Fe-doped $CoCr_2O_4$, Ceram. Int. 44 (2018) 15446–15452.
[13] L. Xie, H.G. Zhang, H.L. Huang, Y.L. Lu, J.Q. Yu, M.H. Li, X.Q. Tang, C. Wang, Coexistence of magnetization reversal and exchange bias in Mn-substituted $CuCrO_2$, J. Alloy. Compd. 772 (2019) 703–709.
[14] J. Nogues, D. Lederman, T.J. Moran, I.K. Schuller, Positive exchange bias in FeF_2-Fe bilayers, Phys. Rev. Lett. 76 (1996) 4624–4627.
[15] L.L. Lei Wang, X. Zhang, M.L. Zhang, Z.C. Zhong, G.H. Rao Zhong, Tunable reversals of magnetization and exchange bias of perovskite YbCr1-Fe O3 (x = 0–0.15), Ceram. Int. 45 (2019) 6143–6148.
[16] G.H. Lei Wang, X. Rao, L.L. Zhang, S.W. Zhang, Q.R. Yao Wang, Reversals of magnetization and exchange-bias in perovskite chromite $TmCrO_3$, Ceram. Int. 42 (2016) 10171–10174.
[17] B.M. Wang, Y. Liu, P. Ren, B. Xia, K.B. Ruan, J.B. Yi, J. Ding, X.G. Li, L. Wang, Large exchange bias after zero-field cooling from an unmagnetized state, Phys. Rev. Lett. 106 (2011) 077203.
[18] L. Xie, H.G. Zhang, Zero-field cooled exchange bias and magnetization reversal in $La_{1.5}Sr_{0.5}Co_{0.4}Fe_{0.6}MnO_6$, Curr. Appl. Phys. 18 (2018) 261–266.
[19] D. Deng, J. Zheng, D. Yu, B. Wang, D. Sun, M. Avdeev, Z. Feng, C. Jing, B. Lu, W. Ren, S. Cao, J. Zhang, Cooling field tuned magnetic phase transition and exchange bias-like effect in $Y_{0.9}Pr_{0.1}CrO_3$, Appl. Phys. Lett. 107 (2015) 102404.
[20] L.N. Bezmaternykh, S.N. Sofronova, N.V. Volkov, E.V. Eremin, O.A. Bayukov, D.A. Velikanov, I.I. Nazarenko, Magnetic properties of $Ni_3B_2O_6$ and $Co_3B_2O_6$ single crystals: magnetic properties of $Ni_3B_2O_6$ and $Co_3B_2O_6$, Phys. Status Solidi B 249 (2012) 1628–1633.
[21] L.N. Bezmaternykh, E.M. Kolesnikova, E.V. Eremin, S.N. Sofronova, N.V. Volkov, M.S. Molokeev, Magnetization pole reversal of ferrimagnetic ludwigites $Mn_{3-x}Ni_xBO_5$, J. Magn. Magn. Mater. 364 (2014) 55–59.
[22] S.N. Sofronova, L.N. Bezmaternykh, E.V. Eremin, I.I. Nazarenko, N.V. Volkov, A.V. Kartashev, E.M. Moshkina, The superexchange interactions and magnetic ordering in low-dimentional ludwigite Ni 5 GeB 2 O 10, J. Magn. Magn. Mater. 401 (2016) 217–222.
[23] K. Bluhm, H. Muller-Buschbaum, Synthesis and structure of Ni5.33Ta0.67B2O10 and Ni_5.33Nb0.67B_2O_{10}, Solis State ion. 43 (1990) 1–5.
[24] A. Harres, M. Mikhov, V. Skumryev, A.M.H. de Andrade, J.E. Schmidt, J. Geshev, Criteria for saturated magnetization loop, J. Magn. Magnetic Mater. 402 (2016) 76–82.
[25] O.A. Bayukov, A.F. Savitskii, The prognostication possibility of some magnetic properties for dielectrics on the basis of covalency parameters of ligand-cation bonds, Phys. Stat. Sol. ((B)) 155 (1989) 249–255.
[26] O.A. Bayukov, A.F. Savitskii, Fiz. Tverd. Tela 36 (1994) (1994) 1923.
[27] P.W. Anderson, New approach to the theory of superexchange interactions, Phys. Rev. 115 (1959) 2–13.
[28] M.V. Eremin, Fiz. Tverd. Tela 24 (1982) 423.
[29] V. Yu, N.V. Knyazev, I.I. Kazak, S.N. Nazarenko, N.D. Sofronova, J. Rostovtsev, A. Bartolome, S.G. Ovchinnikov Arauzo, Effect of magnetic frustrations on magnetism of the Fe3BO5 and Co3BO5 ludwigites, J. Magn. Magn. Mater. 474 (2019) 493–500.
[30] J. Owen, J.H.M. Thornley, Covalent bonding and magnetic properties of transition metal ions, Rep. Prog. Phys. 29 (1966) 675–728.
[31] H.A. Weakliem, Optical Spectra of Ni2+, Co2+, and Cu2+in Tetrahedral Sites in Crystals, J. Chem. Phys. 36 (1962) 2117–2140.